RSC Advances

RSC Advances

ARTICLE

Development of One-Step Synthesized LDH Reinforced Multifunctional Poly(amide‑imide) Matrix Containing Xanthene Rings: Study on Thermal Stability and Flame Retardancy

Received 00th January 20xx,
Accepted 00th January 20xx

DOI: 10.1039/x0xx00000x

www.rsc.org/

M. Hajibeygi[a]*, M. Shabanian[b], H. Moghanian[c], H. A. Khonakdar[d], L. Häußler[e]

New exfoliated poly(amide-imide)/Zn-Al layered double hydroxide (LDH) nanocomposites were synthesized by solution intercalation using synthesized organo-modified LDH (OLDH) as nanofiller obtained by one-step method. The designed poly(amide-imide) (PAI) containing bulky xanthene rings in the side chains, aliphatic chains in the main chains and amide groups in the side and main chains was synthesized via direct polycondensation reaction with desired molecular weight. Poly(amide-imide)/LDH nanocomposites (PAINs) were prepared by different contents of OLDH and morphology, mechanical, thermal and flame retardancy of PAINs were studied. The dispersion of OLDH was quantified by X-ray diffraction (XRD) and transmission electron microscopy (TEM) and the results showed a good dispersion for OLDH in the PAI matrix. According to the results of mechanical tests, the tensile strength of PAIN containing 5 mass% of OLDH increased to 70.1 MPa from 57.3 MPa of neat PAI without OLDH addition. The thermogravimetric analysis (TGA) results showed that the addition of OLDH resulted in a substantial increase in the thermal stability of the PAINs. The temperature at 5% weight loss (T5) was increased from 281 °C to 323 °C for PAIN containing 5 mass% of OLDH as compared to neat PAI, as well the char yield enhanced greatly. Significant improvements in flame retardancy performance were observed for the nanocomposites from microscale combustion calorimeter (MCC) (reducing both the heat release rate and the total heat released).

Key words: Poly(amide-imide); nanocomposite; layered double hydroxide; thermal stability; flame retardant; mechanical properties.

a. a Faculty of Chemistry, Kharazmi University, 15719-14911 Tehran, Iran
b. b Faculty of Chemistry and Petrochemical Engineering, Standard Research Institute (SRI), Karaj, P.O. Box 31745-139, Iran
c. c Department of Chemistry, Dezful Branch, Islamic Azad University, Dezful, Iran
d. d Iran Polymer and Petrochemical Institute, P.O. Box 14965/115, Tehran, Iran
e. e Leibniz-Institut für Polymerforschung Dresden e.V., Hohe Strasse 6, D-01069 Dresden, Germany
E-mail: mhajibeygi@khu.ac.ir, mhajibeygi@gmail.com, Phone: +989122391983, Fax: +982188257969

Introduction

Polymer based materials, are now recognized as key components in many significant industries such as automotive, construction, aerospace and electronic due to their outstanding physical and electronic properties, high versatility, cost-effectiveness and portability [1]. The low flame retardancy is one of the main problems with many polymers, which poses a serious threat to human safety and restricts their applications in many areas. In order to overcome this problem, effective methods are needed to add compatible nano-sized flame retardant fillers into polymer matrices [2, 3].

Layered nanostructure materials, has been reported by many studies as one of the potential candidates for polymeric nanocomposite preparation because of their large value of aspect ratio, diameter in nanometer range, thermal and flame retardancy at low concentration [4-7].

Layered double hydroxides (LDHs), also called anionic clays, are considered as a class of clays and they have a promising future in the field of nanocomposites due to their various unique properties not common in layered silicates. LDHs can be prepared from a wide range of various metal combinations and compositions [8]. LDH consists of a stack of positively charged metal hydroxide layers with intercalated counter anions and water molecules [9]. Using LDH as a host matrix has attracted great attention due to high charge density of LDH layers which leads to increased anion exchange capacity [10]. LDH has been widely used in various fields such as catalysts [11], ion exchange hosts [12], drug delivery [13], hydrothermal reactor [14] and fire retardant additives [15, 16]. Recently many researches have been focused on polymer nanocomposites containing LDH [9, 17-19] and synergistic effects were observed in both thermal stability and flame retardancy for formulations containing polymer matrices with modified Mg-Al and Zn-Al LDH as nanofillers [15, 16, 20].

Due to the increasing demand for high-performance polymers as a good candidate for matrices nanocomposites, thermally stable polymers such as polyimide, polyamides and poly(amide-imide) have attracted increasing interest over the past decade [21-23].

Aromatic polyimides are well recognized as a class of high-performance materials due to their thermal stability in addition to electrical and mechanical properties. Therefore, these polymers are widely used in the fields of electrical materials, film-forming materials and composites [24]. One of the problems with high-performance polyimides is their poor solubility or processability. However, these problems can be solved or reduced by introducing some flexible bonds such as aliphatic chains, pendant bulky group [25, 26] and incorporating flexible units such as amide and ester groups in the polyimide chain [27, 28]. In general, PAIs have been widely used with composites, electronic materials, adhesives and fibers. Compared with the polyimides and polyamides, the PAIs have better processability and thermal properties [29, 30].
Among these approaches, it has been recognized that the incorporation of bulky pendent groups restricts the segmental mobility and raises the Tg, whereas solubility is improved by decreasing the packing density and crystallinity [31, 32].

Xanthenes are frequently occurring motifs in a number of natural products and are known for their utility as leuco-dyes [33, 34], pH-sensitive fluorescent materials for the visualization of biomolecules [35] and in laser technologies [36] due to their useful spectroscopic properties. Xanthene derivatives have also been used for synthesis of aromatic polyamides [37], which are characterized as high thermally stable polymers with a favorable balance of physical and chemical properties. Moreover, these compounds have been incorporated into conjugated polymer backbones as conjugation systems, which can enhance the photoluminescence, electroluminescence, and liquid crystallinity of the polymers [38, 39]. It is thus worthwhile to design a xanthene based aromatic diamine as a starting monomer for the preparation of high performance poly(amide-imide) (PAI).

In this work, in order to prepare polymer/LDH nanocomposites, a new PAI containing xanthene ring as a bulky pendent group was designed and synthesized by direct polycondensation reaction. New PAINs were prepared from PAI and different amount of OLDH by solution intercalation method and effect of OLDH on mechanical properties, thermal stability and flame retardancy of developed PAI was described.

Experimental

Materials

Pyromellitic anhydride, 6-aminohexanoic acid, 2-naphthol, 4-hydroxybenzaldehyde, p-toluenesulfonic acid, 1-fluoro-4-nitrobenzene, 3,5-dinitrobenzoyl chloride, N-methyl-2-pyrrolidone (NMP), N,N-dimethylformamide (DMF), palladium charcoal (Pd/C), hydrazine monohydrate, pyridine (Py) and triphenyl phosphite (TPP) from Merck were used without further purification. Commercially available calcium chloride (CaCl2, Merck) was dried under vacuum at 150 °C for 6 h. Zinc nitrate, aluminum nitrate, sodium hydroxide, and sodium dodecylbenzene sulfonate (SDBS) were used for synthesis of organo-modified Zn-Al LDH by one-step route were also obtained from Merck.

Measurements

^{1}H-NMR spectra were recorded by a Bruker 300 MHz instrument (Germany). Fourier transform infrared (FTIR) spectra were recorded on a Perkin-Elmer RXI spectrometer. The KBr pellet technique was applied for monitoring changes in the range of 400-4000 cm-1 with a resolution of 2 cm-1. Vibration transition frequencies were reported in wave number (cm-1). Band intensities were assigned as weak (w), medium (m), shoulder (sh), strong (s) and broad (br).

Inherent viscosity was measured at a concentration of 0.5g/dL in DMF at 25 °C by a standard procedure using a Technico Regd Trad Mark Viscometer.

Molar mass (weight-average ($\overline{M}w$) and number-average ($\overline{M}n$) molecular weights) determination was performed in size exclusion chromatography (SEC) using Agilent Series 1100 (Agilent, USA) system consisting of a pump, degasser and differential refractive index (RI) detector. Two Zorbax PSM Trimodal-S 250 mm x 6.2 mm columns (Rockland Tech, USA) were used. The measurements were performed using a mixed eluent DMAc with 2 vol.% water and 3 g/L LiCl at a flow rate of 0.5 mL/min. The molar mass was calculated after calibration with poly(2-vinylpyrrolidone) standards.

X-ray diffraction (XRD) was performed on Philips X-Pert. Elemental analyses were performed by Vario EL equipment.

The morphological analysis was carried out using a LEO 912 transmission electron microscopy (TEM) operated at room temperature with an acceleration voltage of 120 kV in a bright field illumination.

Mechanical properties were performed at room temperature on a Testometric Universal Testing Machine M350/500 (Mainz, Germany); Rate, 3 mm/min; according to ASTM D882 (standards).

The thermogravimetric analysis (TGA) was done using a TA Instruments TGAQ5000. About 10 mg of samples was heated from room temperature to 800 °C with a heating rate of 10 °C/min in nitrogen atmosphere.

The flame retardancy properties were analyzed by microscale combustion colorimeter (MCC) that is a convenient and relatively new technique. The MCC measurements were repeated three times. The average values along with standard deviations were reported. In this system, about 5 mg samples were heated to 700 °C at heating rate of 1 °C /s in a stream of nitrogen flowing at 80 cm^3/min. The volatile, anaerobic thermal degradation products in the nitrogen gas stream are mixed with 20 cm^3/min stream of 20% oxygen and 80% nitrogen prior to entering a 900 °C combustion furnace.

Monomer synthesis

Synthesis of diamine 1

N-(4-(4-(14H-dibenzo [a, j] xanthen-14-yl)phenoxy) phenyl)-3,5-diaminobenzamide 1 as a diamine compound containing xanthene and amide group was synthesized starting from 2-naphthol and 4-hydroxybenzaldehyde by five step reactions according to previous literature as following [40].

1. Synthesis of 14-(p-hydroxyphenyl)-14H-dibenzo [a,j] xanthene

2.44 g (20 mmol) of 4-hydroxybenzaldehyde, 6.48 g (45 mmol) of 2-naphtol, 0.172 g (1 mmol) of p-toluenesulfonic acid and 120 mL of 1,2-dichloroethane were placed into a 250 mL round-bottomed flask fitted with a magnetic stirrer under N_2 atmosphere. The reaction mixture was heated under reflux using an oil bath for 24 h. Then, the organic solvent was evaporated and a mixture of EtOH/H_2O (3:1) was added to mixture of reaction. The suspension was stirred for 10 min and the precipitate was filtered. The crude product was recrystallized by a mixture of EtOH and water. Yield = 85 %; mp: 216-218 °C.

2. Synthesis of 14-(4-(4-nitrophenoxy) phenyl)-14H-dibenzo [a,j] xanthene

5.61 g (15 mmol) of 14-(p-hydroxyphenyl)-14H-dibenzo [a,j] xanthene, 2.54 g (18 mmol) of 1-fluoro-4-nitrobenzene, 2.76 g (20 mmol) of K_2CO_3 and 50 mL of DMSO were placed into a 250 mL round-bottomed flask fitted with a magnetic stirrer under N_2 atmosphere. The reaction mixture was heated under reflux using an oil bath for 18 h. Then, the reaction mixture was cooled to room temperature, poured into ice-water to form precipitated. The precipitate was filtered, washed with EtOH and then dried at 80 °C. Yield= 87%; mp: 226–228 °C.

3. Synthesis of 4-(4-(14H-dibenzo [a,j] xanthen-14-yl) phenoxy) aniline

5 g (12 mmol) of 14-(4-(4-nitrophenoxy) phenyl)-14H-dibenzo [a,j] xanthene, 0.2 g of palladium on carbon 10 %, 80 mL of ethanol and 40 mL of THF were placed into a 250 mL round-bottomed flask fitted with a magnetic stirrer under N_2 atmosphere. The mixture was warmed and while being stirred magnetically, a mixture solution of 5 mL of hydrazine monohydrate 80 % and 20 mL of ethanol was added dropwise over a 30 min period through the dropping funnel, while keeping the temperature at about 70 °C. After the complete addition, the reaction was continued at reflux temperature for another 2 h. Then, the mixture was filtered to remove the Pd/C, and the filtrate was poured into water. The product was filtered, washed with EtOH, and dried at 80 °C. Yield= 91%. mp: 182-184 °C.

4. Synthesis of N-(4-(4-(14H-dibenzo [a,j] xanthen-14-yl) phenoxy) phenyl)-3,5-dinitrobenzamide

4.65 g (10 mmol) of 4-(4-(14H-dibenzo [a,j] xanthen-14-yl) phenoxy) aniline, 1 mL of triethylamine and 30 mL of dry dimethylacetamide (DMAc) were placed into a 250 mL round-bottomed flask fitted with a magnetic stirrer under N_2 atmosphere. The reaction mixture was cooled in an ice water bath and while being stirred magnetically, a solution of 3,5-dinitrobenzoyl chloride (3.46 g, 15 mmol) in DMAc (20 mL) was added dropwise over a 20 min period. The mixture was stirred in ice bath for 1 h and at room temperature for overnight. The mixture of reaction was poured into 150 mL of water. The precipitate was collected by filtration and washed thoroughly with ethanol and dried at 100 °C. Yield= 93%; mp: 271-273 °C

5. Synthesis of N-(4-(4-(14H-dibenzo [a,j] xanthen-14-yl) phenoxy) phenyl)-3,5-diaminobenzamide

5 gr (7.58 mmol) of the N-(4-(4-(14H-dibenzo [a,j] xanthen-14-yl) phenoxy) phenyl)-3,5-dinitrobenzamide, 0.4 g of Pd/C 10 %, 80 mL of ethanol and 40 mL of THF were placed into a 250 mL round-bottomed flask fitted with a magnetic stirrer under N_2 atmosphere and a dropping funnel, to which 8 mL of hydrazine monohydrate was added dropwise over a period of 30 min at 70 °C. After the complete addition, the reaction was continued at reflex temperature for another 2 h. Then, the mixture was filtered to remove the Pd/C, and the filtrate poured into water. The product was filtered, washed thoroughly with EtOH, and dried at 80 °C. Yield= 88%; mp: 267-268 °C.

Synthesis of diacid 4

6,6'-(1,3,5,7-tetraoxopyrrolo[3,4-f]isoindole-2,6(1H,3H,5H,7H)-diyl)dihexanoic acid 4 as a diacid compound containing long aliphatic chain and imide heterocyclic ring was synthesized by following procedure:

1 g (4.58 mmol) of pyromellitic anhydride 2, 1.2 g (9.17 mmol) of 6-aminohexanoic acid 3, 40 mL of acetic acid were placed into a 100-mL round-bottomed flask fitted with a magnetic

stirrer under N_2 atmosphere. The mixture was stirred at room temperature overnight and refluxed for 4 h. The solvent was removed under reduced pressure, and the residue was dissolved in 100 mL of cold water, then the solution was decanted and 5 mL of HCl 1 M was added. A white precipitate was formed, filtered off, and dried to give 1.85 g (yield= 91%) diacid 4. FT-IR (KBr): 3102 (w), 2929 (m), 1772 (w), 1705 (s), 1585 (s), 1512 (m), 1459 (w), 1388 (s), 1354 (m), 1307 (m), 1148 (m), 1105 (m), 1047 (w), 836 (w), 721 (m) cm^{-1}.

Synthesis of PAI

PAI was synthesized by adding, 1 g of diacid 4 (2.25 mmol), 1.34 g of diamine 1 (2.25 mmol), 0.50 g of calcium chloride, 1.17 mL of triphenyl phosphite (4.50 mmol), 0.36 mL of pyridine (4.50 mmol) and 10 mL of N-methyl-2-pyrrolidone in 100 mL round-bottom flask fitted with a magnetic stirrer under N_2 atmosphere. The reaction mixture was refluxed in an oil bath at 60 °C for 1 h, 90 °C for 3 h, and 120 °C for 6 h. Subsequently, the reaction mixture was poured into 100 mL of methanol and the precipitated PAI was collected by filtration and washed thoroughly with hot methanol. Finally, the product was dried at 70 °C for 12 h inside a vacuum oven to leave 2.21 g (Yield= 98.2%) pale yellow solid PAI. ηinh (Inherent viscosity, Measured at a concentration of 0.5 g/dL in DMF at 25 °C): 0.82 (dL/g). Elemental analysis: calculated for $C_{62}H_{50}N_5O_9$ (1009.36 g/mol), calculated: C, 73.80; H, 4.99; N, 6.94; found: C, 72.54 ; H, 4.90; N, 6.93.

Preparation of organo-modified Zn-Al LDH (OLDH)

The sodium dodecylbenzene sulfonate (SDBS) modified Zn-Al LDH was prepared in one step according to the procedure reported elsewhere [41].

A solution of $Zn(NO_3)_2$ and $Al(NO_3)_3$ (with Zn^{2+}:Al^{3+} equal to 2:1 and a total metal ion concentration of 0.3 M) was added to SDBS solution slowly. During the Preparation of SDBS modified Zn-Al LDH, solution was stirred at 50 °C and the pH value was kept at 10.5 ± 0.2 by adding suitable amount of a solution of sodium hydroxide. After the addition of the metals salt solution, the resulting mixture was stirred at 50 °C for 30 min. Then the temperature was increased to 70 °C and allowed to age for 24 h. Upon cooling final white product was collected by filtration and washed thoroughly with distilled water until a solution with pH=7 was obtained. The product was then dried in an oven at 75 °C.

Preparation of poly(amide-imide)/LDH nanocomposites (PAIN)s

The nanocomposites were synthesized by taking the PAI solution in a flask, followed by the addition of OLDH for particular concentrations. The amount of OLDH was 2, 5 and 8 mass% in the nanocomposites (PAIN 2, PAIN 5 and PAIN 8). To prepare nanocomposite containing 2 mass% OLDH, 1.96 g of the PAI was dissolved in 10 mL DMF, followed by the addition of 0.04 g of OLDH. The reaction mixture was agitated to high speed at 25 °C overnight to disperse OLDH platelets uniformly in the PAI matrix. The nanocomposites were cast by pouring the hybrid solution in Petri dishes and removing the solvent at 80 °C for 10 h and were further dried at 80 °C under vacuum to a constant weight.

Results and discussion

Synthesis of diamine 1

(N-(4-(4-(14H-dibenzo [a,j] xanthen-14-yl) phenoxy) phenyl)-3,5-diaminobenzamide) 1 was synthesized according to previous work.[40] The Diamine 1 containing amide group, xanthene and fused aromatic rings was used as a monomer to synthesis of a new poly(amide-imide).

Synthesis of diacid 4

The diacid 4 containing imide groups and long aliphatic chain was synthesized from pyromellitic anhydride and 6-aminohexanoic acid in acetic acid. The synthetic route of diacid 4 can be seen in Scheme 1.

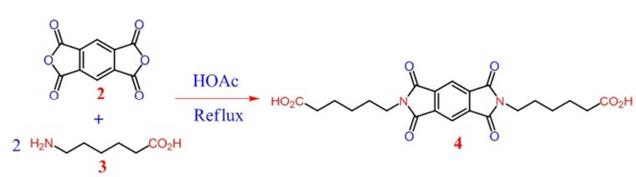

Scheme 1. Synthetic route of diacid **4**

The chemical structure and purity of diacid 4 were confirmed with FTIR and ^{1}H-NMR spectroscopy. The ^{1}H-NMR spectrum of diacid 4 showed peaks that confirm its chemical structure (Fig. 1). The aromatic protons related to pyromellitic aromatic ring appeared at 8.25 ppm. The protons related to carboxylic acid groups appeared at 12 ppm. Five types of aliphatic protons have created five signals in the region of 1-3.75 ppm. Assignments of each proton are also presented in the Figure, and the spectrum agrees well with the proposed diacid 4 structure.

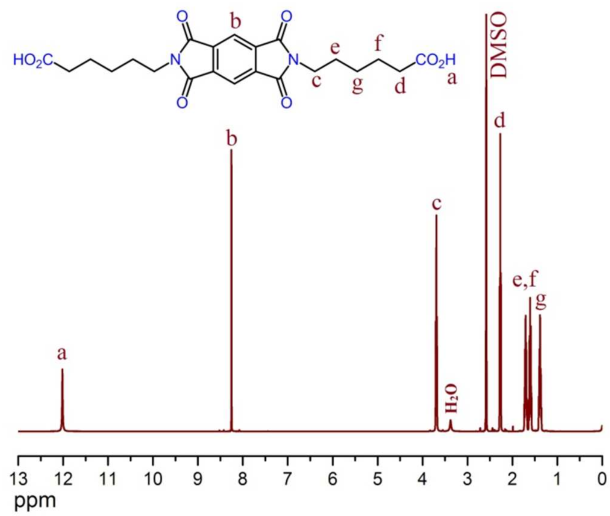

Figure 1. ^{1}H-NMR spectrum of diacid **4**

Polymer synthesis and characterization

Introducing the xanthene rings in the side chain of polymer is a successful approach for improving the processability of aromatic polyamides and polyimides without loss of their important properties such as thermal and mechanical. Furthermore, xanthene skeleton because of their steric bulk improve the solubility of the polymers. Thus, one of the main objectives in this work was synthesis of a new polymer containing 14H-xanthene in the side chain. In order to prepare the matrix of nanocomposites, the Yamazaki method [42] (triphenyl phosphite (TPP)-activated polycondensation) was used to synthesis newly PAI containing long aliphatic chain and xanthene ring in the main chain (Scheme 2). The solubility of this polymer was investigated with 0.01 g of polymeric sample in 2 mL of solvent. Due to presence of bulky pendent group and flexible aliphatic chain in PAI, it had good solubility in organic solvent in room temperature. The polymer was dissolved in polar organic solvents such as dimethyl sulfoxide (DMSO), N,N-dimethyl formamide (DMF), N,N-dimethyl acetamide (DMAc), and N-methyl-2-pyrrolidone (NMP) at room temperature and was insoluble in protic solvents such as methanol, ethanol and water. Also, this synthesized polymer exhibited number-average molecular weight ($\overline{M}n$) and weight-average molecular weight ($\overline{M}w$); 2.8×10^{4} and 5.8×10^{4}, (poly dispersity Index (PDI) =2.07) respectively, as measured by SEC, relative to PVP (Poly(vinylpyrrolidone)) standards.

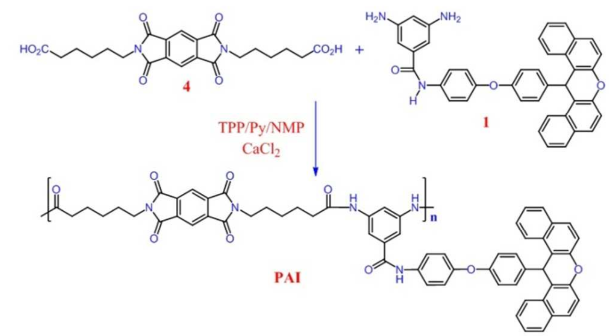

Scheme 2. Synthesis route of **PAI**

The chemical structure of newly synthesized PAI was confirmed by the good agreement of the elemental analysis values with those of the calculated values (see experimental section). In addition, the FTIR and ^{1}H-NMR spectra also supported the formation of PAI having the proposed structure. The ^{1}H-NMR spectrum of the soluble PAI is shown in Figure 2. The disappearance of O-H peak related to carboxylic group and appearing the peaks for the amide groups at 9.93 ppm and 10.18 ppm suggested that polymerization was carried out efficiently. The resonance of aliphatic protons appeared in the range of 1.29-3.56 ppm. The aromatic protons and an aliphatic proton related to CH xanthene appeared in the range of 6.70-8.60 ppm.

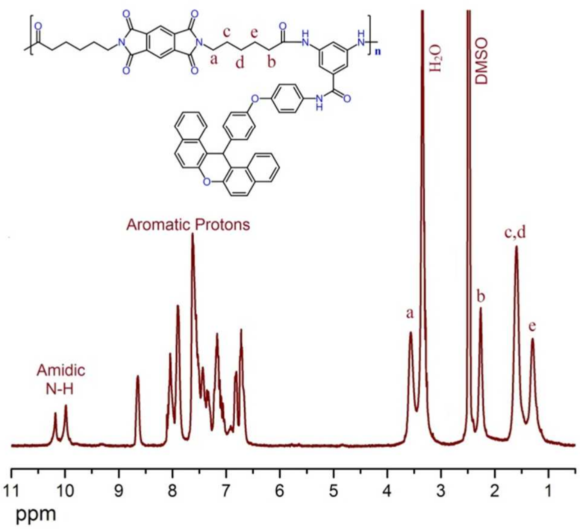

Figure 2. 1H-NMR spectrum of **PAI**

Preparation of PAI/Zn-Al LDH nanocomposites

In general, LDHs are employed to prepare a different organic-inorganic nanohybrid material and have received significant attention. The organic/LDHs nanohybrid have been studied because the resulting intercalation compounds are expected to possess a new nanostructure [43]. In this study SDBS was used as building blocks for efficient prepare of potentially nanohybrid material of OLDH by one-step rout 6. As a possible model, SDBS was considered to be arranged vertically and/or horizontally to the LDH basal layer. In modified LDH, in comparison to neat LDH, the layers of LDH changes from hydrophilic to organophilic and its interlayer space was increased. These phenomena cause enlarge in the d-spacing which facilitates the entry of the polymer molecules between the layers of OLDH for further applications. New PAI/Zn-Al LDH nanocomposites containing 2, 5 and 8 mass% of OLDH were successfully fabricated using modified Zn-Al LDH and PAI in dry DMF through solution intercalation technique (Scheme 3). These new materials are the combinations of synthesized PAI and OLDH blended with each other at ultra fine phase dimensions. The distribution of modified LDH in polymer matrices can lead to physical, morphological, and thermal property enhancements in the resulting nanocomposite materials.

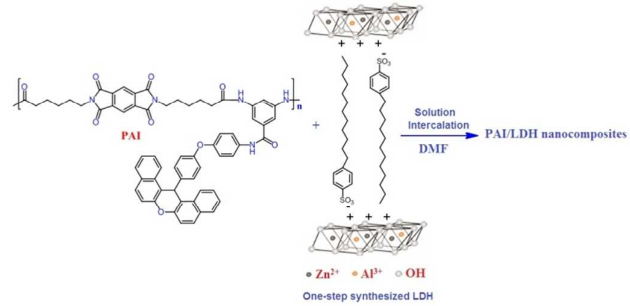

Scheme 3. Preparation of PAI/LDH nanocomposite

Characterization of the PAI/LDH nanocomposites

FTIR Spectra

FTIR spectra of OLDH, PAI and PAINs are shown in Figure 3. In FTIR spectrum of OLDH, a broad and strong band in the range of 3200-3650 cm^{-1} centered at 3475 cm^{-1} related to the O-H stretching vibrations of surface and interlayer water molecule. The band observed near 1601 cm^{-1} related to the bending vibration of water molecule. A strong absorption bands at 2854, 2926 and 2956 cm^{-1} were detected for alkyl groups (CH_3 and CH_2) in SDBS. The characteristic vibration bands were detected for SO3 stretching (symmetric stretching at 1037 cm^{-1} and asymmetric stretching at 1175 cm^{-1}), the benzene group (C–C stretching at 1466 cm^{-1}, C–H in plane bending at 1010 and 1130 cm^{-1}). The bands were recorded below 800 cm^{-1}, especially the sharp and strong characteristic band around 500-800 cm^{-1} were due to the vibration of metal-oxygen bond (Zn-O and Al-O) in the OLDH. These FTIR characteristic bands demonstrated that the SDBS chains had been intercalated into the galleries of Zn-Al LDH.

According to FTIR spectrum of PAI (Fig. 3), absorption bands appeared around 3313 cm^{-1} (N-H), 1769 and 1719 cm^{-1} for the imide ring (asymmetric and symmetric C=O stretching vibration), 1394 cm^{-1} (C-N stretching vibration), 1051 and 728 cm^{-1} (imide ring). The characteristic bands around 2930 cm^{-1} and 3062 cm^{-1} related to C-H aliphatic and aromatic groups in the polymer backbone. Furthermore, a very strong absorption band at 1,240 cm^{-1} in FTIR spectrum of PAI was readily assigned to the C-O vibration of xanthene group and dipheny ether segment; which is normally observed in FTIR spectra of dibenzoxanthenes as the strongest bond.

Figure 3 is also shown the FTIR spectra of PAINs. The characteristic absorption bands for the carbonyl groups around 1770 cm^{-1} related to the asymmetric imide ring stretching vibration and two overlapped around 1719 cm^{-1} related to symmetric imide ring and amide group stretching were observed.

The characteristic absorption bands appeared around 2850-2930 cm^{-1} related to aliphatic groups in OLDH and also PAI. By comparison of these spectra, it can be concluded that the nanocomposits not only have characteristic bands of neat PAI but also have characteristic absorption bands for OLDH. These data, in sum, confirmed the formation of the PAI/LDH nanocomposites.

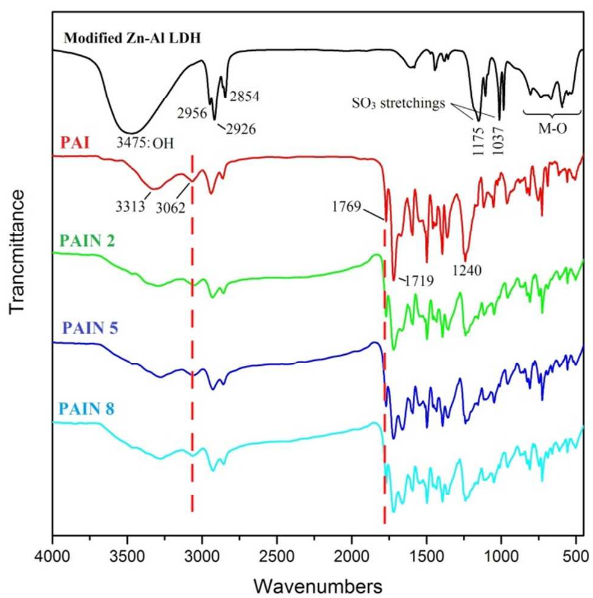

Figure 3. FTIR spectra of OLDH, PAI and PAINs

Structural characterization

Wide angle X-ray scattering (WAXS) and TEM analyses are generally used to analyze the structure and morphology of the layered structure of nanomaterials. X-ray diffraction is one of the most powerful techniques to characterize the layered structure of the polymer nanocomposites, an easy way to access the interlayer spacing of the LDH in polymer nanocomposites. In comparison, TEM analysis gives direct evidence on the dispersion of the nano particles in the nanocomposite

XRD patterns of the one-step prepared OLDH, PAI and PAINs are shown in Figure 4. The interlayer distance of OLDH can be calculated from Bragg diffraction law. The XRD pattern of OLDH points out to a multilayer structure due to the basal diffraction maximum (003) at $2\theta = 3.06°$ (d-spacing: 2.88 nm). In the XRD pattern of PAI, no sharp diffraction signal was observed and this indicated that PAI was amorphous (Fig. 4).

In comparison to basal reflections of OLDH for PAINs, there are almost no peaks corresponding to crystal structure of OLDH. Therefore, a good dispersion for OLDH in the PAI matrix can be expected [44]. In addition, the disappearance of the characteristic reflections related to OLDH in the XRD patterns of PAINs was probably related to the loss of crystalline symmetry in the stacking direction of the hydroxide layers, lowering the number layers of hydroxide and much insertion of the PAI chains into the inter gallery space of OLDH [45].

Disappearance of characteristic reflections in XRD pattern does not always confirm the good dispersion and exfoliated structure in nanocomposites, because XRD is unable to detect regular stacking exceeding 8.8 nm [46], therefore, more direct information can be obtained from TEM. In order to confirm the dispersion of OLDH sheets in PAI matrix, TEM investigations were done on PAIN 2 and PAIN 5 samples and the results are presented in Figure 5. The dark lines represent the LDH layers, whereas the bright area represents the PAI matrix. The TEM images of PAINs showed a good dispersion of OLDH sheets in the PAI matrix, providing a direct evidence of crystal layer exfoliation. This result was supported by the absence of characteristic reflections for PAINs in XRD pattern.

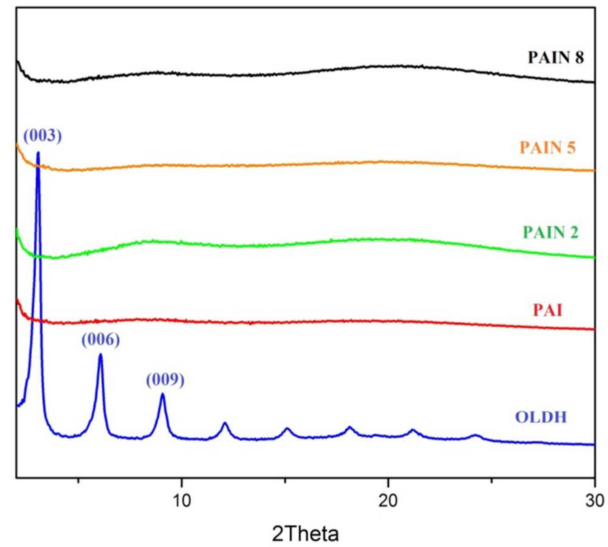

Figure 4. XRD pattern of OLDH, PAI and PAINs

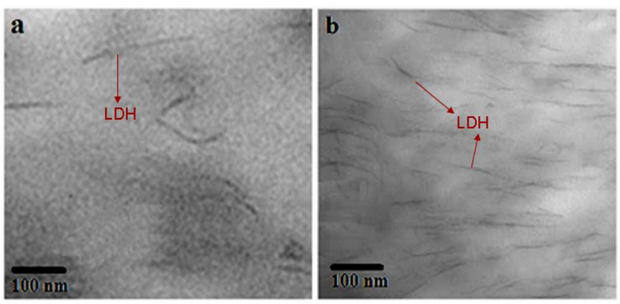

Figure 5. TEM micrographs of a) PAIN 2 and b) PAIN 5

Mechanical properties

Mechanical properties of PAI and PAINs, including the tensile strength and Young's modulus, were measured and the results are listed in Table 1. The relations between tensile strength and Young's modulus of PAINs and OLDH contents are shown in Figure 6. The tensile strengths of PAINs and OLDH contents up to 5 mass% had a linear relationship. The tensile strength increased from 57.3 to 70.1 MPa, which was about 22% higher than that of neat PAI, with the addition 5 mass% of OLDH to neat PAI. This can be attributed to the reinforcement effect attained by the OLDH through random dispersion in the PAI matrix and/or the PAI chains in the nanocomposites were restricted by the OLDH sheets, resulting in the decreased degree of freedom [47].

The Young's modulus values performed the same significant changes of the tensile strength values. The Young's modulus of PAIN 5 was the highest one among them and reached to 3.2 GPa, which was 60% and 39% higher than those of neat PAI and PAIN 2 samples, respectively.

The maximum values in tensile strength and Young's modulus were related to PAIN 5, which then these parameters were decreased with increased OLDH content up to 8 mass% in the PAI matrix. This phenomenon might be due to the increased amount of OLDH in the PAI matrix. The extent of the improvement of mechanical properties depends directly to the dispersion of OLDH. The reason for decrease of tensile strength could be due to aggregation of OLDH that led to its poor dispersion in the PAI matrix [48]. Nevertheless, all of these results showed a good improvement in mechanical properties of PAINs in low concentration of OLDH as compared to neat PAI.

Table 1. Mechanical properties of PAI and PAINs

	TS (MPa)a	YM (GPa)b
PAI	57.3	2.0
PAIN 2	60.2	2.3
PAIN 5	70.1	3.2
PAIN 8	61.9	2.2

a Tensile strength

b Young's modulus

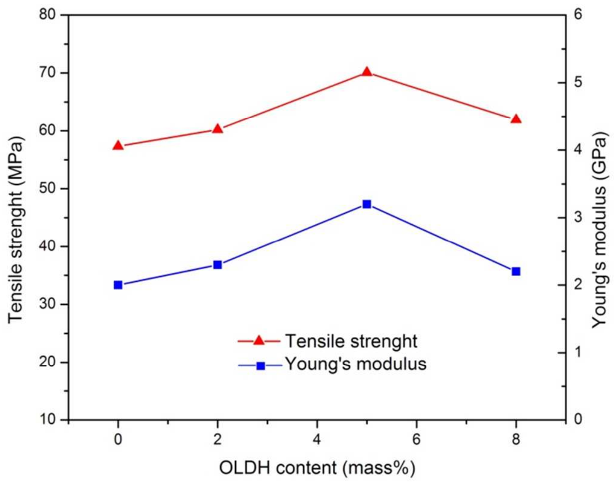

Figure 6. Tensile strength and Young's modulus of PAINs with various OLDH contents

Thermal properties

The TGA thermograms of OLDH, neat PAI and PAINs in nitrogen atmospheres are presented in Figure 7, and the TGA data are summarized in Table 2 that including temperatures at which 5% (T_5), 10% (T_{10}) degradation occur and the residue at 800 °C. According to the TGA thermogram of OLDH, the loss of water molecules and decomposition of SDBS ions in OLDH take place at 100-150 °C and about 200 °C, respectively. The high temperature decomposition of the OLDH takes place with decomposition peak around 450 °C, related to dehydroxylation of the host layers 45. There are many amount of bound water in LDH due to presence of –OH group on the metal hydroxide layers and some molecules of water in the interlayer region. According to most widely reports, there are two stage decomposition processes for LDH: a low temperature dehydration step due to the loss of water molecules between the LDH sheets and a high temperature decomposition step due to the dehydroxylation of the metal hydroxide layer 49.

Figure 7 is also shown the TGA thermogram of PAI and PAINs. The TGA curve exhibited T_5 and T_{10} values 281 °C and 365 °C for neat PAI, respectively. The char yield of PAI was about 39.44%. The thermograms of TGA clearly demonstrated that the thermal degradation temperatures of PAINs were relatively higher than of neat PAI. Considering the TGA curves of nanocomposites it is evident that OLDH has substantial effect on the thermal properties of PAI.

By incorporation of 2 mass% of OLDH to PAI, the T_5 increased by about 30 °C reached to 312 °C. The T10 was also shifted to higher temperature by about 15 °C in PAIN 2 as compared to neat PAI. From Table 2, it can be also observed that increasing OLDH content to 5 mass%, values of T_5, T_{10} and char yield in PAIN 5 reached to 323 °C, 402 °C and 46.4%, respectively. The results suggested that an excess of OLDH in the polymer matrix might restrict the chain mobility as much as disturbing the participation of the PAI chain in the crystallizable unit. This thermal properties is similar to that previously reported for different nanocomposites, and it was there explained by the relative extent of exfoliation and/or delamination processes as a function of the amount of OLDH [6, 50].

The enhanced thermal stability of the PAINs was also attributed to the lower permeability of oxygen and the diffusibility of the degradation products from the bulk of the polymer caused by the exfoliated OLDH in the nanocomposites [51].

By increasing OLDH content to 8 mass% no further improvements was observed with these parameters, specially about T_{10} and char yield, insofar as, the char yield shifted to lower value in PAIN 8 as compared to PAIN 5. The reason could be that LDH has a role for catalytic degradation of PAI and also due to the presence of OLDH sheets aggregates in high concentration in the polymer matrix [52].

DSC was used to determine the glass transition temperature (T_g) values of the samples obtained with a heating rate of 10 °C min-1 under nitrogen atmosphere. The DSC curves of PAI and PAINs are shown in Figure 8 and the results are summarized in Table 2. It was found that addition of OLDH in PAI caused an increase in Tg value. As shown in Table 1, by increasing OLDH content from 2 mass% to 5 mass%, the T_g value increased from 141 °C to 160 °C. These results can be attributed to the well dispersion of OLDH in the PAI matrix. The bulky LDH core might restrict the segmental motion of the PAI chains, and thus higher temperature was required to provide the thermal energy for the occurrence of glass transition in PAINs [53].

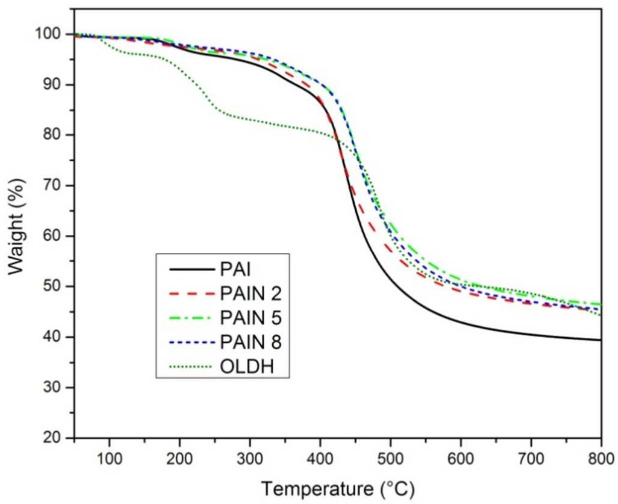

Figure 7. TGA thermograms of OLDH, PAI and PAINs

Table 2. Thermal properties data of PAI and PAINs

Samples	T_5(°C)[a]	T_{10}(°C)[b]	CY (%)[c]	T_g[d](°C)
PAI	281	365	39.44	139
PAIN 2	312	380	45.3	141
PAIN 5	323	402	46.4	160
PAIN 8	334	402	45.5	157

[a] Temperature at 5% weight loss. [b] Temperature at 10% weight loss. [c] CY: Char yield, Weight percentage of material left after TGA analysis at a maximum temperature of 800 °C. [d] Glass transition temperature (T_g) data were recorded by DSC at a heating rate of 10 °C min^{-1}.

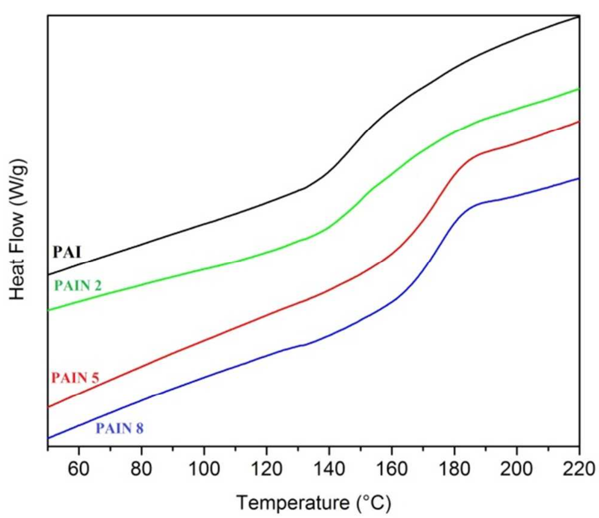

Figure 8. DSC curves of PAI and PAINs

Flammability properties by MCC

Microscale combustion calorimeter (MCC) measures the flammability of materials on milligram quantities and is a small scale flammability testing technique to screen polymer flammability prior to scale-up and is a convenient and relatively new technique, developed in recent years. It was regarded as one of the most effective methods for investigating the combustion properties of polymer materials [54, 55]. The parameters measured from MCC were the heat release rate (HRR) (calculated from the oxygen depletion measurements), the total heat release (THR) (given by integrating the HRR curve) and the heat release capacity (HRC) (obtained by dividing the sum of the peak HRR by the heating rate).

The peak HRR (pHRR) values of PAINs decrease with the increasing OLDH content. As shown in Figure 9 and Table 3, neat PAI undergoes a sharp heat release rate region, and exhibited a peak heat release rate (pHRR) of 175.8 W/g. It was obvious that the pHRR values of both PAIN 2 and PAIN 5 were lower than that of neat PAI. pHRR of PAIN 2 and PAIN 5, were 146.1 W/g and 137.2 W/g, respectively, indicated an improvement in flame retardancy of material. This reduction in heat release rate may be related to the change in the mass loss rate with the increasing OLDH content, which decomposes and releases the vapor of water, cooling the pyrolysis area at the combustion surface.

The total heat release (THR) calculated from the area under the HRR curve is also an important parameter for flame hazard evaluation. Compared to the THR value of 13.5 $KJ.g^{-1}$ in neat PAI, PAIN 2 and PAIN 5 gave 10.2 and 9.9 $KJ.g^{-1}$, respectively. This suggested that the lower HRR and THR of nanocomposites and that the enhanced flame retardancy of PAINs is due to modifications taking place in the condensed phase during polymer combustion 56.

HRC is another important parameter applied to predict flame retardancy of materials 57. As shown Table 3, it can be observed that neat PAI gives the highest HRC of 207 J g^{-1} K^{-1}, while the PAINs showed lower HRC values, indicating that the flame safety of the materials was improved.

According to MCC and TGA results, PAIN 5 had the best improvement thermal stability and flame retardant properties. Since the TGA data showed the high char yield with OLDH loading 5 mass% in PAI, the flame retardant properties may also be due to the formation of char. This char insulates the burning of polymer and decreases the amount of heat transferred to the polymer in combustion 16.

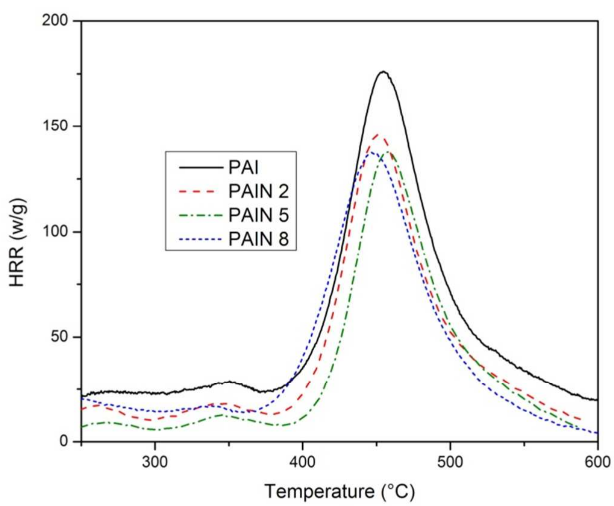

Figure 9. HRR curves of PAI and PAINs

Table 3. Data Recorded in MCC Measurements

Samples	pHRR [W/g][a]	THR [Kj/g][b]	HRC [J/g K][c]
PAI	175.8 ± 2.8	13.5 ± 0.4	207 ± 7.6
PAIN 2	146.1 ± 1.3	10.2 ± 0.4	172 ± 5.4
PAIN 5	137.2 ± 1.4	9.9 ± 0.4	166 ± 2.6
PAIN 8	137.0 ± 1.3	13.2 ± 0.3	156 ± 4.5

[a] Heat release rate. [b] Total heat release. [c] Heat release capacity

Conclusions

New multifunctional poly(amide-imide) containing xanthene rings, long aliphatic chains and amide groups in the side chain and main chain with good yield and desired molecular weight was synthesized trough direct polycondensation reaction. Due to the presence of bulky pendent group in the PAI chains, the newly synthesized PAI had good solubility in organic solvents. New poly(amide-imide)/LDH nanocomposites with three compositions of the OLDH were prepared via solution intercalation method. TEM and XRD results have revealed the formation of exfoliated OLDH in the PAI matrix. Addition of OLDH increased the tensile modulus and tensile strength of the nanocomposites for 2 and 5 mass% content of OLDH as compared to neat PAI. Thermal degradation results showed that the addition low concentrations of OLDH in the PAI matrix significantly increase the thermal stability and char yields of the resulting PAINs. The MCC analysis suggested that presence of OLDH imposes a positive effect on the flame retardancy of neat PAI and decrease pHRR and THR of the nanocomposites. By increasing the concentration of OLDH content up to 5 mass%, the PAINs showed further improvements of flame retardancy. All of the results revealed that incorporation of OLDH was very efficient in improving the mechanical properties, thermal stability and flame retardancy of PAI.

References

1. Y. Gao, J. Wu, Q. Wang, C. A. Wilkie and D. O'Hare, Journal of Materials Chemistry A, 2014, 2, 10996-11016.

2. A. B. Morgan and C. A. Wilkie, Flame Retardant Polymer Nanocomposites, Wiley, 2007.

3. C. J. Hilado, Flammability Handbook for Plastics, Fifth Edition, Taylor & Francis, 1998.

4. S. Sinha Ray and M. Okamoto, Progress in Polymer Science, 2003, 28, 1539-1641.

5. V. Katiyar, N. Gerds, C. B. Koch, J. Risbo, H. C. B. Hansen and D. Plackett, Polymer Degradation and Stability, 2010, 95, 2563-2573.

6. M. Shabanian, N. Basaki, H. A. Khonakdar, S. H. Jafari, K. Hedayati and U. Wagenknecht, Applied Clay Science, 2014, 90, 101-108.

7. H.-W. Wang, R.-X. Dong, C.-L. Liu and H.-Y. Chang, Journal of Applied Polymer Science, 2007, 104, 318-324.

8. B. Kutlu, P. Schröttner, A. Leuteritz, R. Boldt, E. Jacobs and G. Heinrich, Materials Science and Engineering: C, 2014, 41, 8-16.

9. D.-Y. Wang, A. Leuteritz, B. Kutlu, M. A. d. Landwehr, D. Jehnichen, U. Wagenknecht and G. Heinrich, Journal of Alloys and Compounds, 2011, 509, 3497-3501.

10. M. S.-P. Lopez, F. Leroux and C. Mousty, Sensors and Actuators B: Chemical, 2010, 150, 36-42.

11. Q. Wang and D. O'Hare, Chemical Reviews, 2012, 112, 4124-4155.

12. F. Millange, R. I. Walton, L. Lei and D. O'Hare, Chemistry of Materials, 2000, 12, 1990-1994.

13. A. C. S. Alcantara, P. Aranda, M. Darder and E. Ruiz-Hitzky, Journal of Materials Chemistry, 2010, 20, 9495-9504.

14. Q. Wang, S. V. Y. Tang, E. Lester and D. O'Hare, Nanoscale, 2013, 5, 114-117.

15. C. Manzi-Nshuti, J. M. Hossenlopp and C. A. Wilkie, Polymer Degradation and Stability, 2009, 94, 782-788.

16. C. Nyambo, P. Songtipya, E. Manias, M. M. Jimenez-Gasco and C. A. Wilkie, Journal of Materials Chemistry, 2008, 18, 4827-4838.

17. D.-Y. Wang, A. Das, A. Leuteritz, R. Boldt, L. Häußler, U. Wagenknecht and G. Heinrich, Polymer Degradation and Stability, 2011, 96, 285-290.

18. S. Lv, W. Zhou, H. Miao and W. Shi, Progress in Organic Coatings, 2009, 65, 450-456.

19. P. J. Purohit, D.-Y. Wang, F. Emmerling, A. F. Thünemann, G. Heinrich and A. Schönhals, Polymer, 2012, 53, 2245-2254.

20. D.-Y. Wang, A. Das, A. Leuteritz, R. N. Mahaling, D. Jehnichen, U. Wagenknecht and G. Heinrich, RSC Advances, 2012, 2, 3927-3933.

21. M. Shabanian, N.-J. Kang, D.-Y. Wang, U. Wagenknecht and G. Heinrich, RSC Advances, 2013, 3, 20738-20745.

22. S. Mallakpour and M. Dinari, Polymer, 2013, 54, 2907-2916.

23. K.-L. Wang, Y.-L. Liu, I. H. Shih, K.-G. Neoh and E.-T. Kang, Journal of Polymer Science Part A: Polymer Chemistry, 2010, 48, 5790-5800.

24. M. K. Ghosh and K. L. Mittal, Polyimides: Fundamentals and Applications, CRC Press LLC, 1996.

25. D.-J. Liaw, K.-L. Wang, Y.-C. Huang, K.-R. Lee, J.-Y. Lai and C.-S. Ha, Progress in Polymer Science, 2012, 37, 907-974.

26. L. Shao, T.-S. Chung, S. H. Goh and K. P. Pramoda, Journal of Membrane Science, 2005, 256, 46-56.

27. M. Hajibeygi and M. Shabanian, Polymer International, 2014, 63, 514-520.

28. S. Shabbir, S. Zulfiqar, Z. Ahmad and M. I. Sarwar, Polymer Degradation and Stability, 2010, 95, 1251-1259.

29. D.-J. Liaw and W.-H. Chen, Polymer Degradation and Stability, 2006, 91, 1731-1739.

30. C.-P. Yang, R.-S. Chen, K.-S. Hung and E. M. Woo, Polymer International, 2002, 51, 406-416.

31. E. M. Maya, A. E. Lozano, J. de Abajo and J. G. de la Campa, Polymer Degradation and Stability, 2007, 92, 2294-2299.

32. T. Kurosawa, A.-D. Yu, T. Higashihara, W.-C. Chen and M. Ueda, European Polymer Journal, 2013, 49, 3377-3386.

33. S. Hatakeyama, N. Ochi, H. Numata and S. Takano, Journal of the Chemical Society, Chemical Communications, 1988, 1202-1204.

34. G. Mehta and Y. Venkateswarlu, Journal of the Chemical Society, Chemical Communications, 1988, 1200-1202.

35. H.-S. Lv, J. Liu, J. Zhao, B.-X. Zhao and J.-Y. Miao, Sensors and Actuators B: Chemical, 2013, 177, 956-963.

36. G. Harichandran, S. D. Amalraj and P. Shanmugam, Journal of Molecular Catalysis A: Chemical, 2014, 392, 31-38.

37. T. Li, S. R. Sheng, M. H. Wei, C. Chen and C. S. Song, Chinese Chemical Letters, 2010, 21, 1247-1250.

38. Y. Morisaki, T. Murakami and Y. Chujo, Macromolecules, 2008, 41, 5960-5963.

39. Y. Morisaki, T. Murakami, T. Sawamura and Y. Chujo, Macromolecules, 2009, 42, 3656-3660.

40. H. Moghanian, A. Mobinikhaledi and Z. Baharangiz, J Polym Res, 2014, 21, 1-16.

41. D.-Y. Wang, F. R. Costa, A. Vyalikh, A. Leuteritz, U. Scheler, D. Jehnichen, U. Wagenknecht, L. Häussler and G. Heinrich, Chemistry of Materials, 2009, 21, 4490-4497.

42. N. Yamazaki, M. Matsumoto and F. Higashi, Journal of Polymer Science: Polymer Chemistry Edition, 1975, 13, 1373-1380.

43. M. S. Gasser, Colloids and Surfaces B: Biointerfaces, 2009, 73, 103-109.

44. M. Herrero, P. Benito, F. M. Labajos, V. Rives, Y. D. Zhu, G. C. Allen and J. M. Adams, Journal of Solid State Chemistry, 2010, 183, 1645-1651.

45. M. Kotal, T. Kuila, S. K. Srivastava and A. K. Bhowmick, Journal of Applied Polymer Science, 2009, 114, 2691-2699.

46. X. Kornmann, H. Lindberg and L. A. Berglund, Polymer, 2001, 42, 1303-1310.

47. Y.-C. Wang, S.-C. Fan, K.-R. Lee, C.-L. Li, S.-H. Huang, H.-A. Tsai and J.-Y. Lai, Journal of Membrane Science, 2004, 239, 219-226.

48. S. Zulfiqar and M. I. Sarwar, Solid State Sciences, 2009, 11, 1246-1251.

49. E. Kanezaki, Materials Research Bulletin, 1998, 33, 773-778.

50. L. Qiu, W. Chen and B. Qu, Polymer, 2006, 47, 922-930.

51. F. R. Costa, M. Abdel-Goad, U. Wagenknecht and G. Heinrich, Polymer, 2005, 46, 4447-4453.

52. H. Acharya, S. K. Srivastava and A. K. Bhowmick, Composites Science and Technology, 2007, 67, 2807-2816.

53. L. Hu, Y. Yuan and W. Shi, Materials Research Bulletin, 2011, 46, 244-251.

54. M. Shabanian, N.-J. Kang, D.-Y. Wang, U. Wagenknecht and G. Heinrich, Polymer Degradation and Stability, 2013, 98, 1036-1042.

55. D.-Y. Wang, A. Leuteritz, Y.-Z. Wang, U. Wagenknecht and G. Heinrich, Polymer Degradation and Stability, 2010, 95, 2474-2480.

56. C. Manzi-Nshuti, P. Songtipya, E. Manias, M. M. Jimenez-Gasco, J. M. Hossenlopp and C. A. Wilkie, Polymer, 2009, 50, 3564-3574.

57. Y. Shi, T. Kashiwagi, R. N. Walters, J. W. Gilman, R. E. Lyon and D. Y. Sogah, Polymer, 2009, 50, 3478-3487.